Electronic Supplementary Material (ESI) for Inorganic Chemistry Frontiers.

Supporting Information for

Photocatalyst with enhanced Schottky effect and efficient electron-transfer channel by assembling Ni-WC heterojunction nanoparticles on g-C_3N_4 for highly efficient removal of chlorophenols

Qi Wang, Qian Liu, Yuan-Yuan Ma*, Hao-Xue Bi, Jing Du*, Zhan-Gang Han*

Hebei Key Laboratory of Organic Functional Molecules, National Demonstration Center for Experimental Chemistry Education, Testing and Analysis Center, College of Chemistry and Materials Science, Hebei Normal University, Shijiazhuang, Hebei 050024, P. R. China.

*Corresponding author email: mayy334@hebtu.edu.cn; duj622@hebtu.edu.cn; hanzg116@126.com;

CONTENTS

1. Additional experimental section

2. Supplementary figures

3. Supplementary tables

1. Additional experimental section

1.1 Chemicals and Materials

Nickel chloride ($NiCl_2 \cdot 6H_2O$, AR, 99%), tris (AR, 99%), 1,3,5-benzenetricarboxylic acid (H_3BTC, AR, 99%) and urea (AR, 99%) were supplied by Alfa Aesar. 1,4-Benzoquinone (AR, 99%), isopropanol (AR, 99%), alcohol (AR, 99%), acetone (AR, 99%), EDTA-Na_2 (AR, 99%) and ethylenediamine (en, AR,99%) were provided by Tianjin Chemical Technology. *P*-chlorophenol (4-CP, AR, 99%) and *o*-chlorophenol (2-CP, AR, 99%), 2,4-dichlorophenol (2,4-DCP, AR, 99%), 4-chlorophenoxyacetic acid (4-CPA, AR, 99%), 2,4,6-trichlorophenol (2,4,6-TCP, AR, 99%), aniline (AR, 99%), methanol (GR) and $(NH_4)_2S_2O_8$ (AR, 99%) were bought from Aladdin Industrial Inc. (Shanghai, China). All materials were used without any modification. De-ionized (DI) water with a resistivity of 18.2 MΩ cm was used for preparing samples and electrochemical measurements. $[Ni(en)_2(H_2O)_2]_6\{Ni_6(Tris)(en)_3(BTC)_{1.5}(B\text{-}\alpha\text{-}PW_9O_{34})\}_8 \cdot 12en \cdot 54H_2O$ (denoted as $\{Ni_{54}W_{72}\}$) was prepared as reported.[1] The graphitic carbon nitride ($g\text{-}C_3N_4$) was synthesized *via* the pyrolysis method by using urea as the raw material. [2]

1.2 Photocatalytic degradation of 4-CP

A 100 W LED lamp was used as the light source. In a typical reaction, 25 mL 100 $mg \cdot L^{-1}$ of 4-CP solution with 10 mg catalyst was magnetically stirred for 0.5 h under dark to obtain adsorption/desorption equilibrium of 4-CP on the catalyst, then the solution was exposed to visible light. At irradiation time intervals of every 0.5 h, 0.5 mL sample was collected from the reaction system for further analysis. Each sample was passed through a 0.22 μm filter membrane. The removal rate of 4-CP was measured using a high-performance liquid chromatography (HPLC, Agilent Technologies 1200 Series) equipped with a C18 column (150 mm×4.6 mm×5μm) and a UV detector at 278 nm. The mobile phase was 60:40 (V/V) mixture of methanol and water at 1.0 $mL \cdot min^{-1}$. For reusability of Ni-WC/CN, 10 repeated experiments were conducted under the same conditions to the initial experiments. In detail, the conditions for each cycle keep the same as those for the first time. After each cycle, the catalyst was collected by centrifugation and transferred it in a fresh 25 mL 100 $mg \cdot L^{-1}$ of 4-CP solution and stirred for 0.5 h under dark to obtain adsorption/desorption equilibrium. Then, the recycle system was placed under 100 W LED for the next photocatalytic reaction. To evaluate the practical applications prospect of Ni-WC/CN, the photocatalytic experiment was also conducted in a natural lake water system. Specifically, the natural lake water was obtained from Xiyue Lake and filtrated to remove the insoluble impurities. Then the filtrated lake water served as a solvent for the preparation of 100 mg L^{-1} of 4-CP solution. The photocatalytic degradation procedures in natural lake water were similar to the common photocatalytic process. The biological safety of the treated water was evaluated by comparing the chlorophyll variation in the ceratophyllum demersum. 50 mg ceratophyllum demersum tissues were

grinded and immersed in a 5 mL of solution ($V_{ethanol}$:$V_{acetone}$:$^{V_{H_2O}}$ = 4.5:4.5:1), then place it in dark condition for 12 h, finally, the optical density at 660 nm (OD_{660}) was measured to evaluate the growth state of ceratophyllum demersum.

1.3 Theoretical calculation methods

Periodic DFT calculations were conducted by using the Vienna ab initio Simulation Package (VASP) with exchange and correlation potential represented by the PBE approximation. A suitable k-point grid of 4 × 4 × 1 Å was generated with the Monkhorst-Pack algorithm with the kinetic energy cutoff of 450 eV. All calculated results were obtained until the forces and energy were less than 0.03 eV·$Å^{-1}$ and 10^{-6} eV, respectively.

1.4 Characterization

The transmission electron microscope (TEM) images of the synthesized catalysts were recorded on the transmission electron microscope (JEM-F-200, JEOL) operated at an accelerating voltage of 200 kV. Scanning electron microscopy (SEM) used a Quanta 250 FEG. X-ray diffraction (XRD) patterns were collected by using the equipment of Regaku D/Max-2500 diffractometer at 40 kV and 40 mA covering the 2Θ range from 10° to 80° with a Cu Kα radiation and a scanning rate of 6 °·min^{-1}. X-ray photoelectron spectroscopy (XPS) and ultraviolet photoelectron spectroscopy (UPS) were recorded on a Thermo SCIENTIFIC ESCALAB 250 Axis Ultra spectrometer using a monochromatic Al K_α (h□= 1486.6 eV). The binding energies were calibrated using C1s peak of contaminant carbon (284.8 eV). Fourier transform infrared (FTIR) spectra were recorded on a Thermo SCIENTIFIC apparatus. Ultraviolet-visible diffuse reflectance spectra (UV-vis, U-4100, Hitachi) were recorded to characterize the light absorption properties of samples. Photoluminescence (PL) spectra of samples were tested using a fluorescence spectrophotometer (FLS980, Edinburgh). Total organic carbon (TOC) was recorded by a Shimadzu TOC-VCPH analyzer. The metal loadings were determined *via* thermal gravimetric analysis (TGA) under an N_2 flow on a Netzsch DSC214. A multimode atomic force microscope (AFM, OXFORD, MFP-3D) was used to analyze the local work functions and moduli of different phases of the samples by the KPFM techniques. All photoelectrochemical measurements were carried out in a standard three-electrode system on a CHI 760E electrochemical workstation at room temperature. The reference and counter electrodes were the Ag/AgCl and Pt wires, respectively. The measured potential *vs*. Ag/AgCl was converted to the reversible hydrogen electrode (RHE) scale with the Nernst equation. $E_{RHE} = E_{Ag/AgCl} + 0.059\times Ph + E^{\theta}_{Ag/AgCl}$.

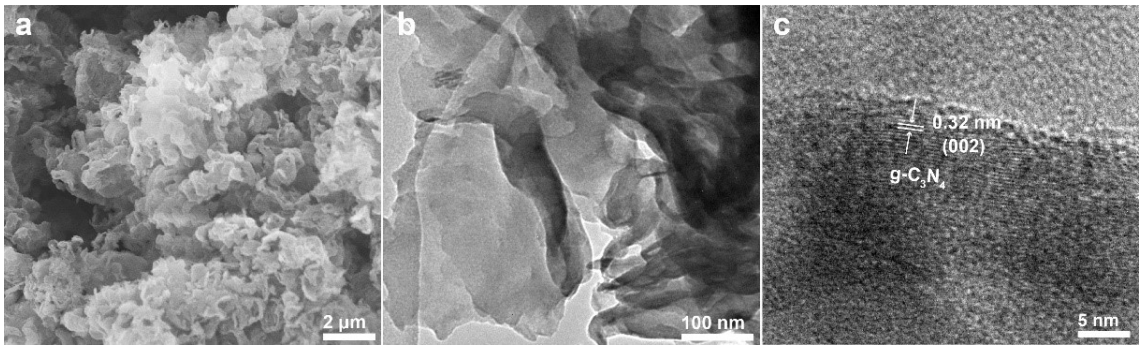

Figure S1. (a) SEM image of g-C_3N_4; (b-c) TEM images of g-C_3N_4.

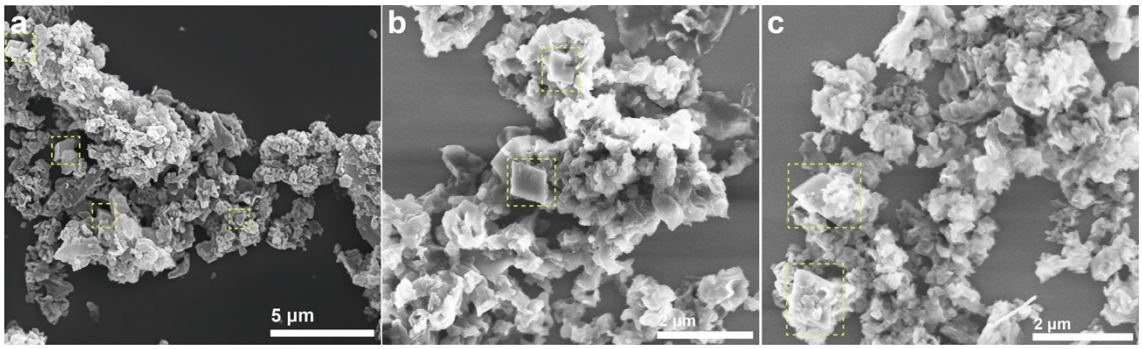

Figure S2. SEM images of $\{Ni_{54}W_{72}\}$/g-C_3N_4.

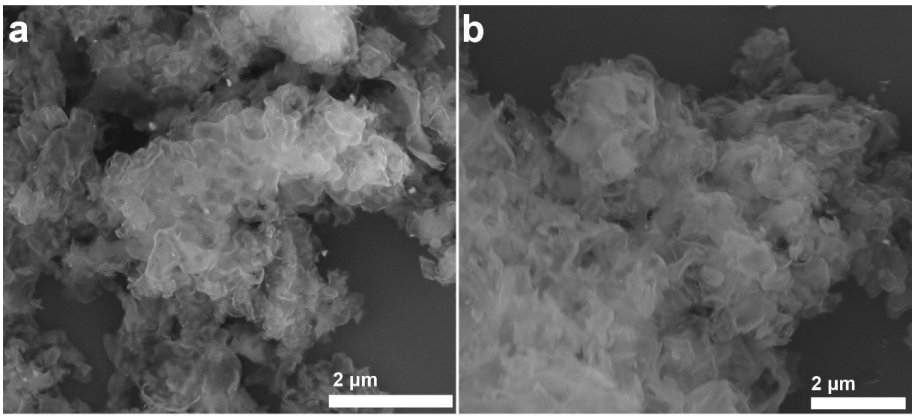

Figure S3. (a-b) SEM images of Ni-WC/CN.

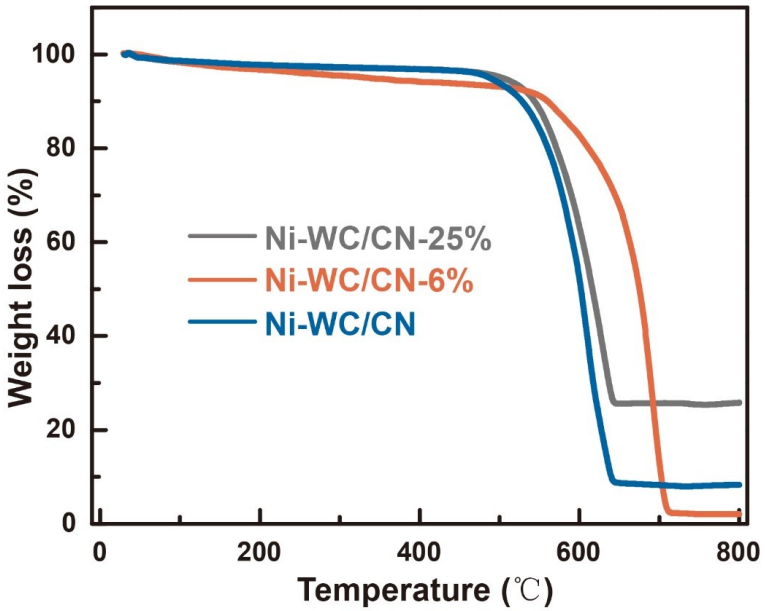

Figure S4. TG curves of Ni-WC/CN, Ni-WC/CN-6% and Ni-WC/CN-25%.

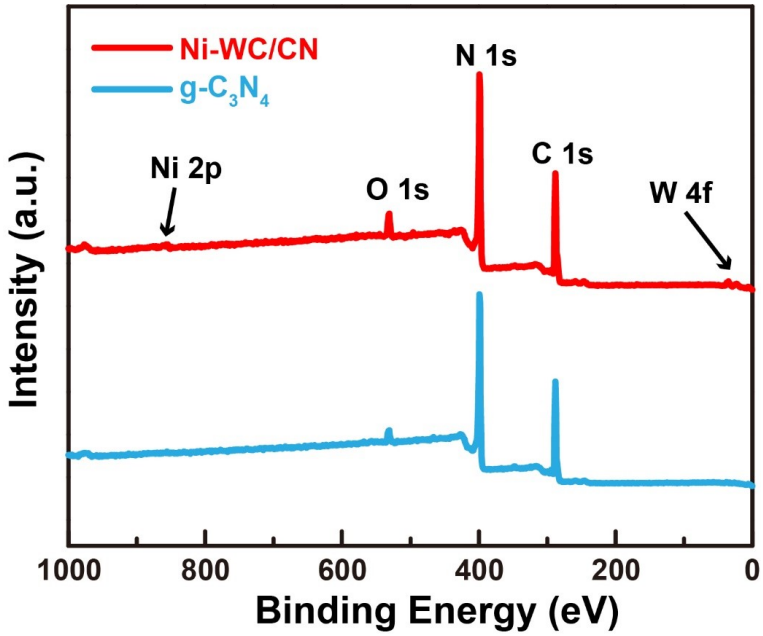

Figure S5. XPS survey spectra of g-C_3N_4 and Ni-WC/CN.

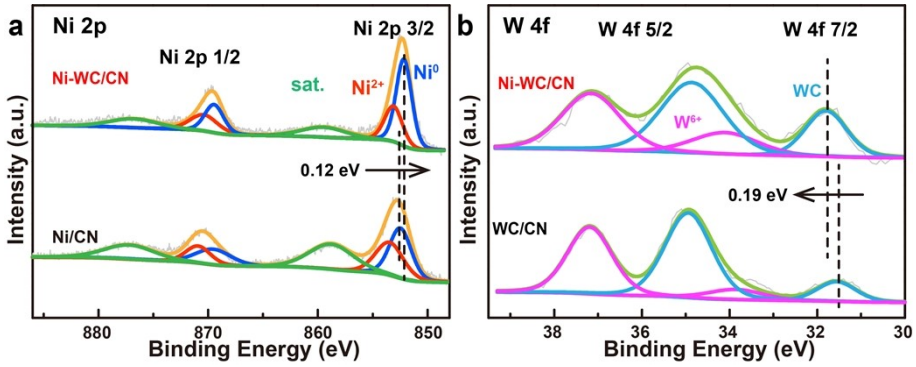

Figure S6. High-resolution XPS spectra of Ni 2p in Ni-WC/CN and Ni/CN; (b) High-resolution XPS spectra of W 4f in Ni-WC/CN and WC/CN.

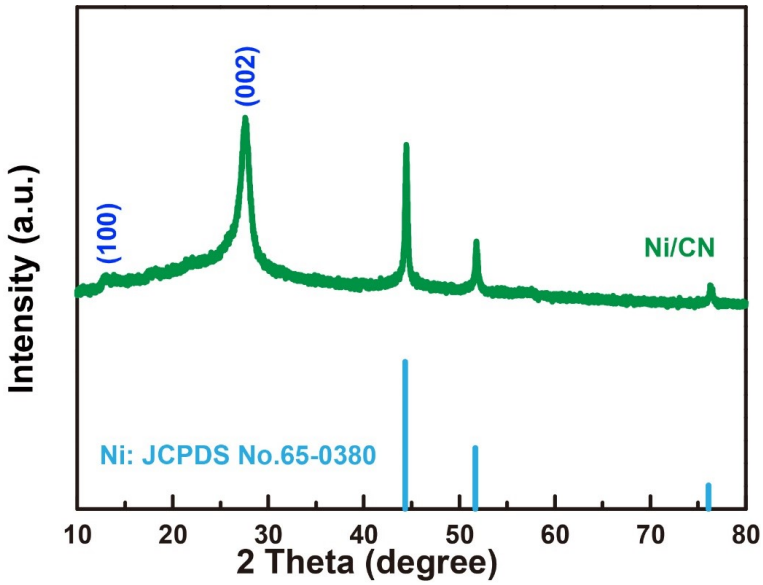

Figure S7. XRD patterns of Ni/CN.

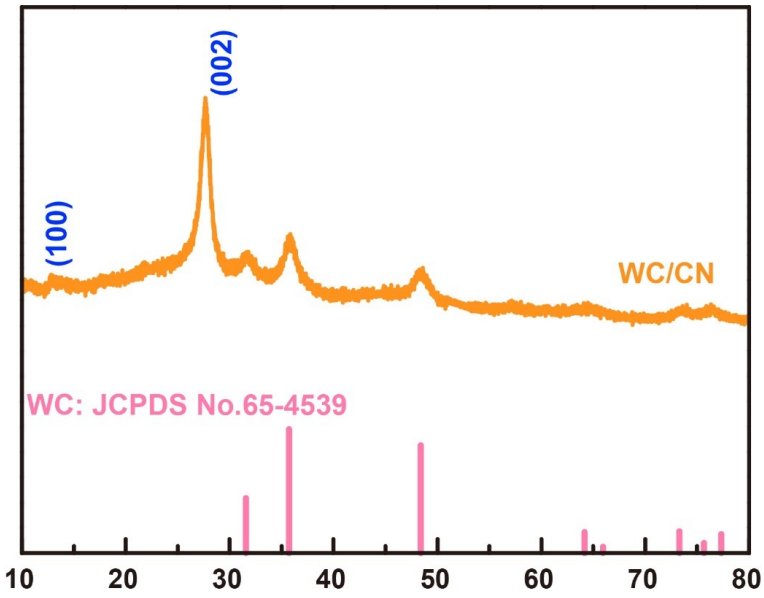

Figure S8. XRD patterns of WC/CN.

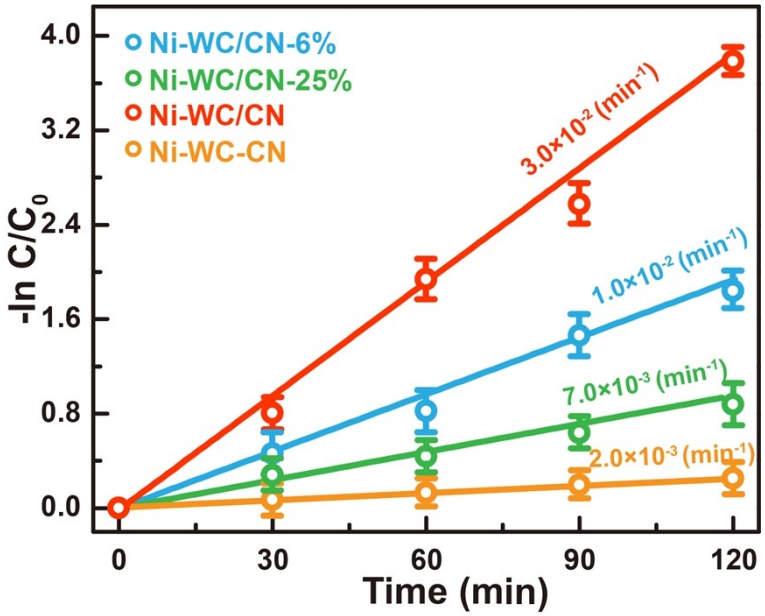

Figure S9. Pseudo-first-order kinetic curves of Ni-WC/CN with different Ni-WC loadings.

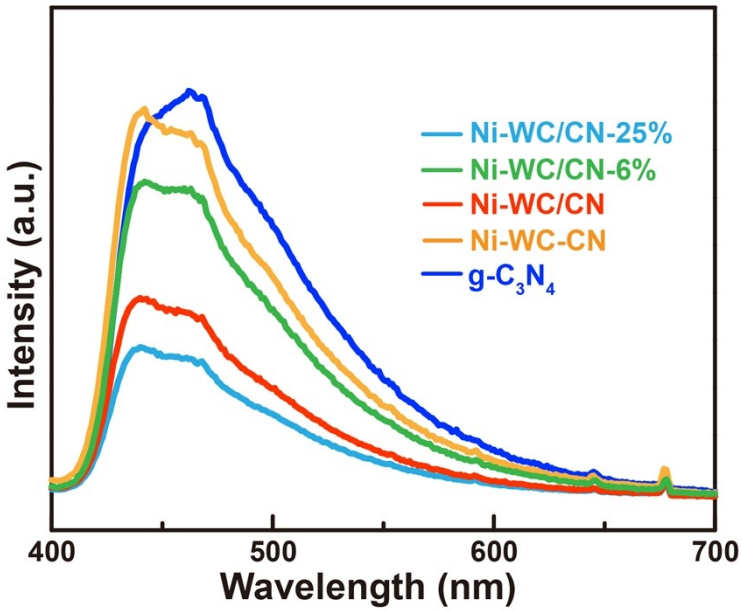

Figure S10. Steady-state PL spectra of g-C_3N_4, Ni-WC-CN, Ni-WC/CN-6%, Ni-WC/CN and Ni-WC/CN-25%.

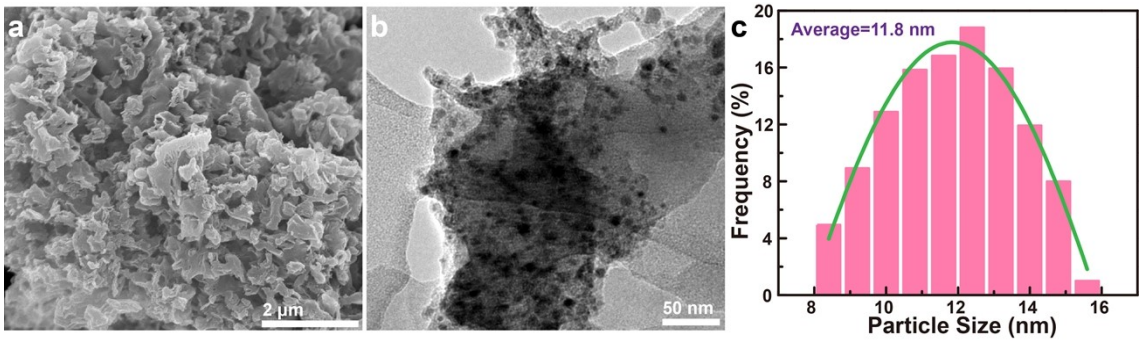

Figure S11. (a) SEM image of Ni-WC/CN-25%; (b) TEM image of Ni-WC/CN-25%; (c) Particle size distribution of Ni-WC hybrid nanoparticles in Ni-WC/CN-25%.

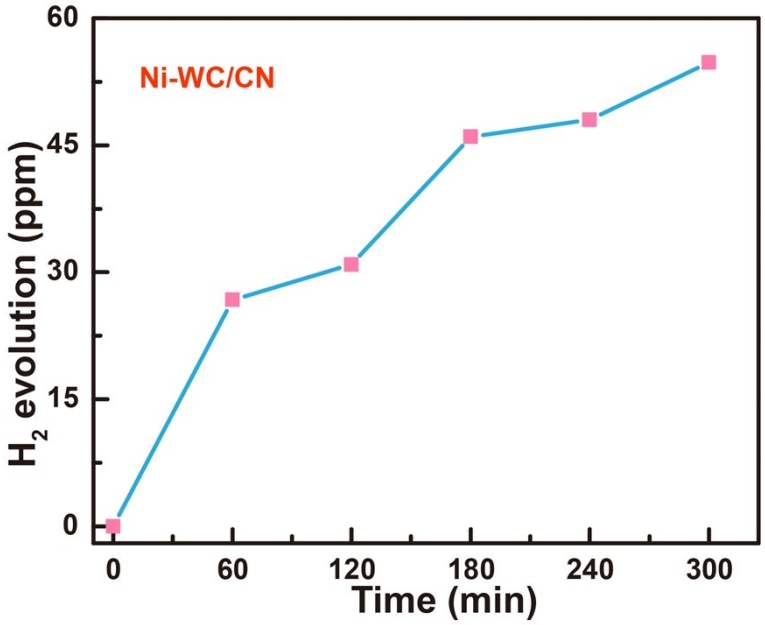

Figure S12. Hydrogen production performance of Ni-WC/CN.

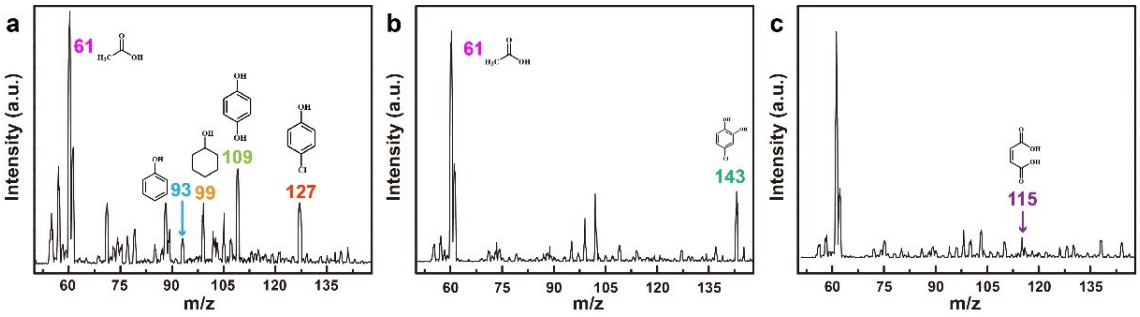

Figure S13. (a) The main intermediate products generated during the process of photocatalytic degradation of 4-CP for 30 min, (b) 60 min and (c) 90 min.

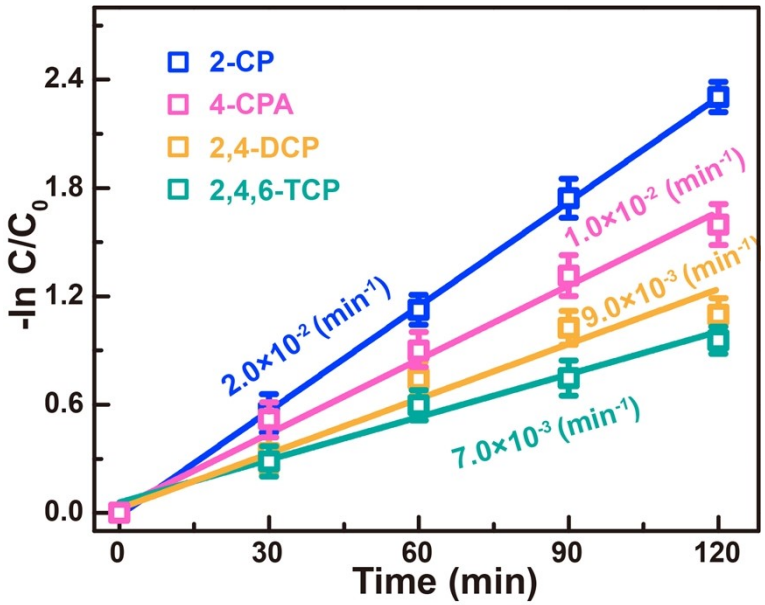

Figure S14. Pseudo-first-order curves of the monochlorophenols, dichlorophenols and trichlorophenols over Ni-WC/CN.

Table S1 The binding energy of C, N, Ni and W in g-C_3N_4, Ni-WC, Ni/CN, WC/CN and Ni-WC/CN

	C-C/C=C	N-C=N	C-N=C	Ni	WC
g-C_3N_4	284.81	288.21	398.51	**/**	**/**
Ni-WC	**/**	**/**	**/**	852.56	32.09
Ni-WC/CN	285.05	287.52	398.72	852.22	31.80
Ni/CN	/	/	/	852.31	/
WC/CN	/	/	/	/	31.6

Table S2 Comparison of the degradation performance of Ni-WC/CN with other g-C_3N_4-based photochemical systems

Photocatalyst	Conditions					
	Catalyst dosage	Illumination	4-CP content	Time (min)	k_{app}(min^{-1})	Ref.
g-C_3N_4/PTCDI-Br	50	300 W Xe lamp	5 mg	60	/	[3]
ZNi-WCO_4/g-C_3N_4	10	500 W Xe lamp	0.1 mg	100	$1.7*10^{-3}$	[4]
$BiVO_4$/g-C_3N_4	10	500 W Xe lamp	0.1 mg	100	$1.3*10^{-3}$	[5]
g-C_3N_4/ZnO	100	λ>420 nm	10^{-5} mol	90	$5.1*10^{-3}$	[6]
$YFeO_3$/g-C_3N_4	50	λ>420 nm	10^{-5} mol	300	/	[7]
ZrO_2/g-C_3N_4	60	300 W Xe lamp	3 mg	120	$3.0*10^{-2}$	[8]
g-C_3N_4/BiOI	100	300 W Xe lamp	1 mg	180	$1.0*10^{-1}$	[9]
g-C_3N_4/ZnO	100	300 W Xe lamp	$2.5*10^{-5}$ mol	40	/	[10]
Ni-WC/CN	**10**	**100 W LED**	**2.5 mg**	**90**	**$3.0*10^{-2}$**	**This work**

Reference

1. S.-T. Zheng, J. Zhang, X.-X. Li, W.-H. Fang and G.-Y. Yang, Cubic polyoxometalate−organic molecular cage, *J. Am. Chem. Soc.*, 2010, **132**, 15102-15103.
2. X. Wang, X. Wang, W. Tian, A. Meng, Z. Li, S. Li, L. Wang and G. Li, High-energy ball-milling constructing P-doped g-C_3N_4/MoP heterojunction with MoN bond bridged interface and Schottky barrier for enhanced photocatalytic H_2 evolution, *Appl. Catal. B: Environ*, 2022, **303**, 120933.
3. J. Liu, D. Han, P. Chen, L. Zhai, Y. Wang, W. Chen, L. Mi and L. Yang, Positive roles of Br in g-C_3N_4/PTCDI-Br heterojunction for photocatalytic degrading chlorophenols, *Chem. Eng. J.*, 2021, **418**, 129492.
4. V. Rathi, A. Panneerselvam and R. Sathiyapriya, Graphitic carbon nitride (g-C_3N_4) decorated $ZnWO_4$ heterojunctions architecture synthesis, characterization and photocatalytic activity evaluation, *Diamond Relat. Mater.*, 2020, **108**, 107981.
5. V. Rathi, A. Panneerselvam and R. Sathiyapriya, A novel hydrothermal induced $BiVO_4$/g-C_3N_4 heterojunctions visible-light photocatalyst for effective elimination of aqueous organic pollutants, *Vacuum*, 2020, **180**, 109458.
6. J. Wang, Y. Xia, H. Zhao, G. Wang, L. Xiang, J. Xu and S. Komarneni, Oxygen defects-mediated Z-scheme charge separation in g-C_3N_4/ZnO photocatalysts for enhanced visible-light degradation of 4-chlorophenol and hydrogen evolution, *Appl. Catal. B: Environ*, 2017, **206**, 406-416.
7. M. Ismael, E. Elhaddad, D. H. Taffa and M. Wark, Solid state route for synthesis of $YFeO_3$/g-C_3N_4 composites and its visible light activity for degradation of organic pollutants, *Catal. Today*, 2018, **313**, 47-54.
8. M. Zarei, Ultrasonic-assisted preparation of ZrO_2/g-C_3N_4 nanocomposites with high visible-light photocatalytic activity for degradation of 4-chlorophenol in water, *Water-Energy Nexus*, 2020, **3**, 135-142.
9. J. Di, J. Xia, S. Yin, H. Xu, L. Xu, Y. Xu, M. He and H. Li, Preparation of sphere-like g-C_3N_4/BiOI photocatalysts via a reactable ionic liquid for visible-light-driven photocatalytic degradation of pollutants, *J. Mater. Chem. A*, 2014, **2**, 5340-5351.
10. N. Kumaresan, M. M. A. Sinthiya, M. Sarathbavan, K. Ramamurthi, K. Sethuraman and R. R. Babu, Synergetic effect of g-C_3N_4/ZnO binary nanocomposites heterojunction on improving charge carrier separation through 2D/1D nanostructures for effective photocatalytic activity under the sunlight irradiation, *Sep. Purif. Technol.*, 2020, **244**, 116356.